Palaeogeography, Palaeoclimatology, Palaeoecology 438 (2015) 256–266

Contents lists available at ScienceDirect

Palaeogeography, Palaeoclimatology, Palaeoecology

journal homepage: www.elsevier.com/locate/palaeo

A record of wet glacial stages and dry interglacial stages over the last 560 kyr from a standing massive stalagmite in Carlsbad Cavern, New Mexico, USA

L. Bruce Railsback [a,*], George A. Brook [b], Brooks B. Ellwood [c], Fuyuan Liang [d], Hai Cheng [e,f], R. Lawrence Edwards [f]

[a] Department of Geology, University of Georgia, Athens, GA 30602-2501, USA
[b] Department of Geography, University of Georgia, Athens, GA 30602-2502, USA
[c] Department of Geology and Geophysics, Louisiana State University, Baton Rouge, LA 70803, USA
[d] Department of Geography, Western Illinois University, 1 University Circle, Macomb, IL 61455, USA
[e] College of Global Environmental Change, Xi'an Jiaotong University, Xi'an, Shaanxi 710049, China
[f] Department of Geology and Geophysics, University of Minnesota, Minneapolis, MN 55455, USA

ARTICLE INFO

Article history:
Received 23 February 2015
Received in revised form 8 August 2015
Accepted 10 August 2015
Available online 18 August 2015

Keywords:
Stalagmite
Carlsbad
Quaternary
Pleistocene
Palaeoclimate
Glacials

ABSTRACT

A horizontal core through a large, standing, stalagmite in Carlsbad Caverns National Park, New Mexico, USA, provides a radiometrically dated record of wetter glacial stages and drier interglacial stages over the last 560 kyr. The stalagmite, the Texas Toothpick, is about 7 m tall and about 3 m wide at its base. Two cores through the stalagmite reveal five distinct matching layers, and the best estimates from twenty U–Th ages indicate that those layers were deposited during MIS 6, 8, 10, 12, and 14, the five glacial periods ending with the Penultimate Glacial Maximum (PGM). Stable isotope data, measurements of remanent magnetism, and petrographic observations combine to suggest that conditions during glacials, the periods in which deposition took place, were significantly wetter than today. On the other hand, the stalagmite's hiatuses seemingly represent conditions during interglacials similar to or drier than today. These results combine with modern climatological observations to suggest 100-kyr-scale alternation between wetter conditions with an increased proportion of winter rainfall from a Pacific source during glacials to drier conditions with largely summer rainfall derived from the Gulf of Mexico during interglacials. The length and continuity of the results confirm that the pattern of wetter glacials and drier interglacials, known previously from studies isolated in time, existed across all of at least the last six glacial cycles. Simple monotonic extrapolation of these findings from cooler wetter glacials of the past and warmer drier interglacials like the present to a warmer climate expected in the coming century suggests that groundwater in the already dry southwestern United States may become even more scarce.

1. Introduction

Records of climate history, like most historical records, collectively provide us with more information about the more recent past than about the more distant past. Thus, within the context of the Quaternary, records from intervals before MIS 5 are scarce, and publications about them constitute only about 6% of the palaeoclimatological literature (Railsback, 2015). Continental records with evidence of a long sequence of glacial and interglacial periods, such as the Tenaghi Philippon record (Tzedakis et al., 2006), Sabana de Bogota pollen record (Dueñas–J., 1979), and Chinese loess records (e.g., Sun et al., 2006), are even more scarce. Among those, there are very few radiometrically-dated records. With that in mind, this paper reports on a large and ancient stalagmite named the Texas Toothpick from Carlsbad Caverns National Park, New Mexico, located in the southwestern United States. Twenty U–Th dates from the Texas Toothpick provide a chronology for a record that extends from Marine Isotope Stage (MIS) 6 to MIS 14 and, combined with a previously published record from the Georgia Giant Stalagmite at Carlsbad (Brook et al., 2006), provides a record extending back through the last six glacial cycles, to about 560 ka BP. The Texas Toothpick record is thus exceptionally ancient and lengthy, and it demonstrates that patterns of climate change from wetter glacials to drier interglacials known either from the last glacial cycle (e.g., Rich, 2013) or from single earlier cycles (e.g., Fawcett et al., 2011) are in fact part of a continuous pattern over at least the last six glacial cycles. This record has implications not only for our understanding of past climate but also for possible climate change in the future.

2. Carlsbad cavern and the Texas Toothpick

Carlsbad Cavern is located in southeastern New Mexico, USA, at 32° 11′ N, 104° 27′ W, roughly 1000 km from the Gulf of Mexico

* Corresponding author. Tel.: +1 706 542 3453; fax: +1 706 542 2425.
E-mail address: rlsbk@gly.uga.edu (L.B. Railsback).

http://dx.doi.org/10.1016/j.palaeo.2015.08.010
0031-0182/

Fig. 1. Map of the southwestern United States and northern Mexico showing the location of Carlsbad Cavern (filled circle) and other locations discussed in Section 5.2.2. Circles (both open and filled) indicate locations at which wetter glacials and/or drier interglacials have been inferred; arrows indicate locations at which influence of westerly winds of the Polar Jet Stream during glacials has been inferred. The boundaries of the four deserts shown are from Figs. 5.1 and 5.2 of MacMahon and Wagner (1985).

and 1300 km from the Pacific Ocean (Fig. 1). The cave lies in the northern Chihuahuan Desert, which extends from San Luis Potosi in Mexico to central New Mexico in the United States. Data from the U.S. National Weather Service indicate that average annual precipitation is 342 mm/year, more than half of which falls in the summer months from June through September. This rainfall occurs as part of the Mexican Monsoon (Douglas et al., 1993) or North American Monsoon (Adams and Comrie, 1997), although it is beyond the northern limit of the North American monsoon in the global-scale context shown in Fig. 1 of Wang (2009). The summer rainfall accompanies winds dominantly from the southeast that bring moisture from the Gulf of Mexico (Feng et al., 2014, their Fig. 1).

Carlsbad Cavern is the focal point of Carlsbad Caverns National Park, a World Heritage Site that hosts both Carlsbad Cavern and Lechuguilla Cave. The Park is located in the Guadalupe Mountains, and Carlsbad Cavern is developed in reefal facies of the Capitan Limestone of Permian age. Carlsbad Cavern alone has about 48 km of passage and a total vertical extent of 317 m (Burger, 2009). Much of the cave is more than 200 m below the land surface and cave entrance, resulting in a travel time for water from the surface to the cave that is on the order of decades (Chapman et al., 1992).

Carlsbad Cavern contains speleothems of diverse form and mineralogy (e.g., Table 1 of Thrailkill, 1977), including some that are exceptionally large. The cave has for decades been the site of research about the origin and nature of speleothems (e.g., Black, 1953; Thrailkill, 1968, 1977; Hill, 1973; Folk and Assereto, 1976; Gonzalez and Lohmann, 1988). More recently, stalagmites in the cave have been studied as records of climate change from the Last Glacial Maximum to the Holocene (Polyak and Asmerom 2001; Polyak et al., 2004; 2012; Brook et al., 2006; Asmerom et al., 2013).

Carlsbad Cavern has at least two speleothems named "Texas Toothpick". One is a long stalactite, and the other, which is the focus of this paper, is a stalagmite about 7 m tall and about 3 m wide near its base (Fig. 2). The flanks of the lower half of the stalagmite slope at 55° to 70°, whereas the flanks of the upper half slope at 75° to 90° and have a lower drapery-like fringe half way up the stalagmite. That fringe at the midpoint of the stalagmite (Fig. 2A) suggests that the latest phase of deposition, which is hypothesized to have occurred during the last (Late Pleistocene) glacial cycle (Fig. 2B), did not extend to the stalagmite's base.

3. Methods

3.1. Coring of the stalagmite

In summer 1983, two parallel side-by-side horizontal cores designated "CA" and "CC" were drilled from the Texas Toothpick stalagmite (Fig. 2). The drill rig was powered by two 12 V marine batteries hooked in series. The drill was mounted on a collapsible aluminum frame with four telescoping legs and three adjustable front pads to position the frame against the stalagmite. Drilling was accomplished using a series of short, threaded 5 cm-internal-diameter steel pipes; the edge of one had rectangular plates, impregnated with industrial diamonds, welded to the pipe, with spaces between the plates, to form a drill bit. A padded cable was wrapped around the stalagmite and tightened to hold the drilling frame in position during coring, and pressure, using bungee

Table 1
^{230}Th dating results from Core CA of the Texas Toothpick stalagmite. The error is 2σ error.

Sample ID	Distance in core (cm)	Calcite color[a]	Mass (g)	^{238}U (ppb)	^{232}Th (ppt)	δ^{234}U measured[b]	[^{230}Th/^{238}U] activity[c]	[^{230}Th/^{232}Th] ppm	Age (ka) uncorrected	Age (ka) corrected[d]	$\delta^{234}U_{initial}$ corrected[e]	Status[f]
TXT 92-95-1	0.6	B	0.145	221.8 ± 0.7	169 ± 5	1000.8 ± 6.6	1.60469 ± 0.00883	34674 ± 1004	144.9 ± 1.7	144.9 ± 1.7	1506.4 ± 12.3	A
TXT 92-95-2	3.4	B	0.160	218.9 ± 0.5	41 ± 4	993.5 ± 5.4	1.62706 ± 0.00579	143023 ± 15167	149.7 ± 1.3	149.8 ± 1.3	1515.9 ± 10.0	A
TXT 89-92-1	10.3	B	0.176	290.2 ± 0.8	31 ± 4	989.3 ± 5.6	1.63781 ± 0.00632	252451 ± 32180	152.2 ± 1.4	152.2 ± 1.4	1502.2 ± 10.5	A
TXT 85-88-1	17.5	B	0.183	315.9 ± 0.9	85 ± 4	986.6 ± 6.2	1.65041 ± 0.00649	101562 ± 4581	154.9 ± 1.5	154.9 ± 1.5	1527.4 ± 11.6	A
TXT 82-85-1	23.4	B	0.193	350.8 ± 1.3	32 ± 4	971.7 ± 6.7	1.64822 ± 0.00885	301352 ± 34406	157.0 ± 2.0	156.9 ± 2.0	1513.1 ± 13.5	A
TXT 79-82-1	31.4	B	0.191	331.8 ± 1.2	73 ± 4	941.2 ± 6.7	1.62481 ± 0.00930	122575 ± 6215	157.8 ± 2.1	157.8 ± 2.1	1469.0 ± 13.7	A
TXT 79-82-2	31.8	W	0.183	232.0 ± 0.6	16 ± 4	946.9 ± 6.1	1.54353 ± 0.00684	361321 ± 84142	142.5 ± 1.4	142.5 ± 1.4	1415.6 ± 10.7	R
TXT 79-82-3	32.3	W	0.169	85.0 ± 0.2	52 ± 4	865.6 ± 7.0	1.76959 ± 0.00671	47407 ± 3736	208.4 ± 2.9	208.4 ± 2.9	1558.7 ± 18.0	R
TXT 79-82-4	33.5	A	0.173	249.1 ± 0.6	34 ± 4	708.8 ± 5.5	1.71140 ± 0.00632	205669 ± 24255	249.1 ± 3.9	249.1 ± 3.9	1431.5 ± 19.7	A
TXT 79-82-5	37.2	A	0.181	288.7 ± 0.8	29 ± 4	707.7 ± 5.4	1.72540 ± 0.00626	287308 ± 38674	256.0 ± 4.1	256.0 ± 4.1	1457.4 ± 20.6	A
TXT 79-82-6	38.4	W	0.145	96.1 ± 0.2	48 ± 5	558.3 ± 5.3	1.74500 ± 0.00689	58059 ± 5858	452.4 ± 23.1	452.3 ± 23.1	2001.0 ± 144.9	R
TXT 76-79-1	40.5	A	0.170	260.7 ± 0.7	41 ± 4	550.4 ± 5.1	1.65402 ± 0.00669	173683 ± 17396	335.1 ± 9.1	335.1 ± 9.1	1417.0 ± 40.3	A
TXT 73-76-1	48.2	A	0.175	405.4 ± 1.2	52 ± 4	547.0 ± 5.1	1.65926 ± 0.00688	215329 ± 16660	344.8 ± 10.0	344.8 ± 10.0	1447.2 ± 44.9	A
TXT 70-73-1	56.9	A	0.174	358.3 ± 1.0	46 ± 4	540.6 ± 5.0	1.64296 ± 0.00740	210543 ± 18307	336.4 ± 9.7	336.4 ± 9.7	1397.1 ± 42.0	A
TXT 67-70-1	66.6	A	0.162	389.6 ± 1.6	90 ± 4	531.8 ± 5.8	1.65271 ± 0.01195	118286 ± 5760	359.3 ± 17.0	359.3 ± 16.9	1466.1 ± 77.2	A
TXT 64-67-2	77.6	A	0.148	492.6 ± 1.7	56 ± 5	537.2 ± 5.3	1.65035 ± 0.00781	239775 ± 20211	348.8 ± 11.4	348.8 ± 11.4	1437.4 ± 50.7	A
TXT 64-67-1	79.4	A	0.146	245.1 ± 0.7	285 ± 5	416.3 ± 5.0	1.55122 ± 0.00642	21973 ± 379	451.5 ± 25.9	451.5 ± 25.9	1488.5 ± 122.5	A
TXT 61-64-1	87.0	A	0.206	458.4 ± 1.9	90 ± 3	403.3 ± 5.6	1.54494 ± 0.01065	129325 ± 4950	488.4 ± 50.0	488.4 ± 50.0	1600.0 ± 279.2	A
TXT 55-58-4	103.1	A	0.167	432.0 ± 1.3	89 ± 4	410.6 ± 4.8	1.54521 ± 0.00707	124364 ± 5890	456.5 ± 28.0	456.5 ± 28.0	1488.8 ± 133.6	A
TXT 55-58-3	103.8	W	0.184	165.1 ± 0.4	54 ± 4	399.4 ± 4.6	1.54553 ± 0.00690	77861 ± 5467	512.6 ± 42.3	512.6 ± 42.3	1696.5 ± 242.0	R
TXT 55-58-2	104.0	W	0.185	125.4 ± 0.3	102 ± 4	334.9 ± 5.2	1.47864 ± 0.00622	30107 ± 1123	749.2 ± 6651.9	749.2 ± 6651.0	–	R
TXT 55-58-1	104.7	A	0.155	213.7 ± 0.8	91 ± 5	314.4 ± 6.9	1.43445 ± 0.00744	55673 ± 2766	553.5 ± 93.1	553.5 ± 93.1	1499.4 ± 584.5	A
TXT 40-43-1	160.0	A	0.207	347.7 ± 1.4	48 ± 3	313.5 ± 5.4	1.43132 ± 0.00852	171171 ± 12065	541.2 ± 76.5	541.2 ± 76.5	1444.1 ± 428.9	A
TXT 15-18-4[g]	208.1	A	0.162	243.7 ± 0.9	29 ± 4	549.7 ± 8.4	1.65809 ± 0.00880	228738 ± 33768	340.0 ± 14.1	340.0 ± 14.1	1434.8 ± 64.5	A
TXT 15-18-3	209.1	W	0.252	201.6 ± 0.6	40 ± 3	553.2 ± 6.5	1.72350 ± 0.00862	141974 ± 9756	422.2 ± 22.9	422.2 ± 22.9	821.0 ± 131.3	R
TXT 15-18-2	209.8	W	0.219	163 ± 1	57 ± 3	669.4 ± 8.9	1.72806 ± 0.00962	81389 ± 4574	280.7 ± 8.3	280.7 ± 8.3	1478.2 ± 40.9	R
TXT 15-18-1[g]	210.9	A	0.158	910.9 ± 4.1	240 ± 5	694.7 ± 6.0	1.71160 ± 0.01173	106928 ± 2123	256.6 ± 6.4	256.6 ± 6.4	1433.1 ± 29.5	A

Decay constants are 9.1705×10^{-6} yr^{-1} for ^{230}Th, 2.8221×10^{-6} yr^{-1} for ^{234}U, and 1.55125×10^{-10} yr^{-1} for ^{238}U.

[a] A = amber; B = beige; W = white.

[b] $\delta^{234}U = ([^{234}U/^{238}U]_{activity} - 1) \times 1000$.

[c] $[^{230}Th/^{238}U]_{activity} = 1 - e^{-\lambda 230 T} + (\delta^{234}U_{measured} / 1000)[\lambda_{230} / (\lambda_{230} - \lambda_{234})](1 - e^{-(\lambda 230 - \lambda 234) T})$, where T is the age.

[d] Corrected ^{230}Th ages assume the initial ^{230}Th/^{232}Th atomic ratio of $4.4 \pm 2.2 \times 10^{-6}$. Those are the values for a material at secular equilibrium, with the bulk earth ^{232}Th/^{238}U value of 3.8. The errors are arbitrarily assumed to be 50%.

[e] $\delta^{234}U_{initial}$ was calculated based on ^{230}Th age (T), i.e., $\delta^{234}U_{initial} = \delta^{234}U_{measured} \times e^{\lambda 234 \times T}$, and T is corrected age.

[f] A = accepted; R = rejected for reasons discussed in Section 4.2.

[g] These two ages are not used in Fig. 6 because they are from the right side of the stalagmite, but they confirm that the visible symmetry of the Texas Toothpick's layers is a symmetry of chronology.

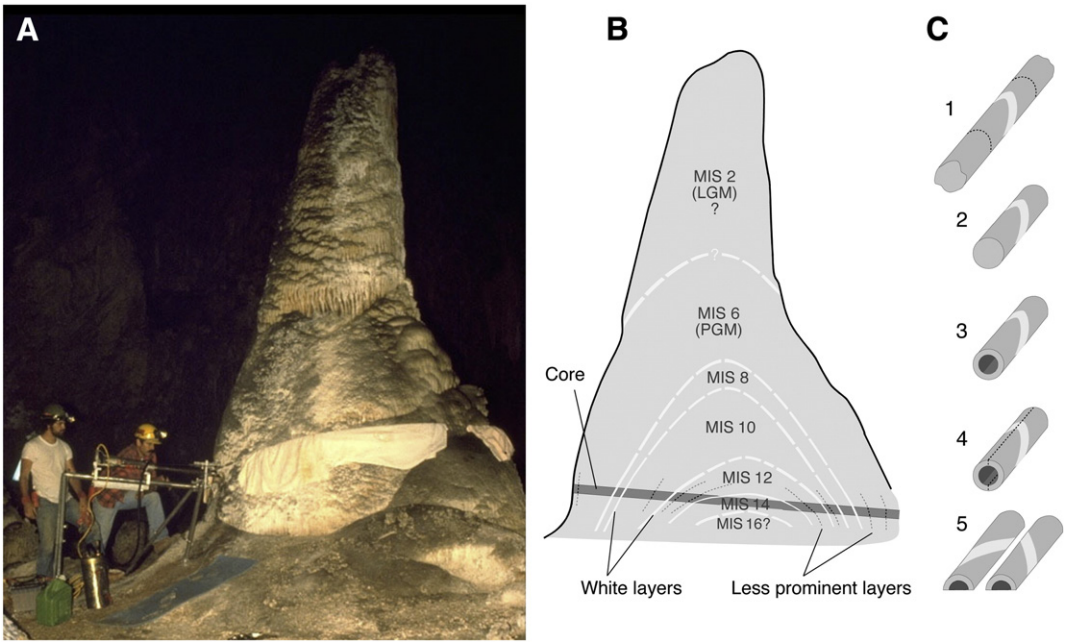

Fig. 2. The Texas Toothpick. A. Photograph of the Texas Toothpick and the drilling operation to recover the core that is the subject of this paper. Brooks B. Ellwood and UGA graduate student Mark Earley are shown. B. Sketch of the Texas Toothpick core (gray bar with white stripes) and inferred internal structure of the entire stalagmite shown in cross-section. C. Sketches showing how the original core (1) was cut transversely (2), cored for paleomagnetic analysis (3), and then cut lengthwise vertically into two pieces (4–5).

straps, was applied during the drilling process. Water was pumped along the drill for lubrication and to flush out fine material produced by the drilling process.

Cores CA and CC were 46 mm in diameter as drilled. A secondary core 24 mm in diameter was drilled from the center of each of the original cores for paleomagnetic analysis. The remaining hollow cylinders were sectioned lengthwise vertically (Fig. 2C). Core CA was the focus of this study.

3.2. Analytical methods

Our sampling strategy for age-dating focused on two objectives: dating of the white layer-bounding zones and dating of the sequence as a whole, with samples from throughout the core. The results discussed in Section 4.2 reveal that the first objective was unattainable, but the ages from the second one provide a chronology for the stalagmite. U–Th ages were determined in the Minnesota Isotope Laboratory of the University of Minnesota using inductively coupled plasma mass spectrometry (ICP-MS, Thermo-Finnigan Element) according to the method described in Edwards et al. (1987) and Shen et al. (2002). The dating results were calculated using half-lives determined by Cheng et al. (2000) and reported with analytical errors of 2σ of the mean.

Our sampling strategy for stable isotope analysis focused on two objectives. One was generation of a series of samples throughout the core, with a spacing of 1.0–1.5 cm. The second was more detailed sampling in white zones, where faster-paced change was expected; the spacing there was 0.1–0.6 cm. Samples for stable isotope analysis were collected using a dental drill and analyzed at the University of Alabama Stable Isotope Laboratory using a GasBench-IRMS system by implementing methods similar to those described by Debajyoti and Skrzpek (2007). Uncertainties were about 0.1‰ for both $\delta^{18}O$ and $\delta^{13}C$. Results are reported relative to the VPDB (Vienna Peedee Belemnite) standard.

Remanent magnetism was measured on 181 samples from Cores CA and CC, using the cryogenic magnetometer in the laboratory of Prof. Victor Schmidt at the University of Pittsburgh. Stepwise a.f. demagnetization was performed at 5 mT and at 10 mT steps to 50 mT on all samples with a natural RM greater than 4×10^{-5} A/m. Mineralogy was determined by petrographic examination of thin sections.

4. Results

4.1. General characteristics

Core CA consists entirely of calcite with a fabric of elongate calcite crystals that are as much as 0.8 mm wide and tens of mm long. Much of the calcite in the interior of the stalagmite is amber in reflected light, but within the amber calcite are distinct bands of white that are 4 to 12 mm thick and are perpendicular or nearly perpendicular to the calcite crystals. Four bands slope away from the center of the stalagmite, less steeply in the center and more steeply at the flanks, and four more bands are positioned symmetrically on the opposite side of the stalagmite (Fig. 3). These eight white bands in the core thus appear to be four distinct layers marking the pattern of growth of the stalagmite (Fig. 2B). Beyond the outermost and thus latest white band is an interval of amber calcite only 4 mm thick and then an outermost interval of beige calcite that is 31 cm thick. Within this outermost beige calcite is one more, but thinner (2 mm), white band. Core CC shows the same distribution of amber, white, and beige calcite.

The white bands of the Texas Toothpick cores are distinct in their color, physical strength, petrography, translucence, and remanent magnetization (RM). During drilling, the core often parted along the white bands, suggesting lesser strength there. Petrographically, the white bands consist of the same elongate calcite crystals as the amber and beige calcite, but in the white bands those crystals are pitted with small (typically 0.02–0.05 mm) vacuities and contain even smaller particles that are effectively opaque (Fig. 4). The white zones are less translucent than the amber calcite, a pattern similar to that observed in a brown-and-white stalagmite from China previously described by Railsback et al. (2014). Of the 181 samples from Cores CA and CC on which RM was measured, only 30 samples had RM greater than 4×10^{-5} A/m, and almost all of these were from white bands. These characteristics combine to suggest that the white bands are zones of

Fig. 3. Core CA recovered from the Texas Toothpick using the drilling system shown in Fig. 2. This image shows the two halves of the core laid flat and thus shows both sides of the core, as the result of the longitudinal sectioning of the core sketched in Part 5 of Fig. 2C. The top of the original core is the horizontal line separating the two halves. The dark vertical lines crossing the core are the cuts made perpendicular to the core, as shown in Part 2 of Fig. 2C. The lower half of the image shows the core from the side, with its top up, whereas the upper half of the image shows the core inverted vertically, as suggested by Part 5 of Fig. 2C. Coring passed from one side of the Texas Toothpick to the other, so that the oldest section of the core is in the middle (MIS 14), and MIS 12, 10, 8 and 6 are represented in both the proximal and distal halves of the core. Note that coring in this manner allows both sides of the stalagmite to be sampled for redundancy.

non-deposition that were corroded by condensation and on which dust settled to deposit the magnetic particles causing the RM observed in those white bands. Type E layers showing evidence of dissolutional erosion (Railsback et al., 2013) are not present in the white bands or elsewhere in the Texas Toothpick cores.

4.2. Radiometric ages and chronology

Radiometric U/Th ages from amber and beige calcite in Core CA range from 144.9 to 553.5 ka, in a sequence in which there are no reversals if analytical uncertainty is taken into account (Fig. 5; Table 1). The ages cluster at 149–158 ka, 249–257 ka, 336–359 ka, 451–488 ka, and 541–553 ka, where each cluster is in brown or beige calcite that is between or beyond the four large bands of white calcite. The best estimates for these ages correspond with MIS 6, 8, 10, 12, and 14, which are the Penultimate Glacial Maximum and the four glacial maxima before that (Fig. 6). However, the uncertainties for the ages in the 541–553 ka cluster are so large they could be anywhere from MIS 12 to MIS 16. Growth rates generally decrease from the center of the stalagmite to its edge, and most markedly within MIS 6, its outermost interval.

Results from dating of white calcite include ages as great as 749 ka, and they include ages older than those of underlying brown calcite, producing age reversals. Concentrations of ^{238}U in six of the seven samples from white calcite are less than 210 ppb, whereas ^{238}U concentrations in all of the samples from beige and amber calcite exceed that value. These results suggest loss of U from the white calcite bands, consistent with the hypothesis above of corrosion of that calcite during periods of non-deposition. Therefore, we have not incorporated ages from white calcite in the chronology shown in Fig. 5 nor in the compilation of ages shown in Fig. 6.

The reliable ages that we have obtained from beige and amber calcite, combined with our understanding that the four white calcite bands represent periods of non-deposition, lead to the conclusion that the cores record five periods of growth during glacial Marine Isotope Stages 6, 8, 10, 12, and 14, with four major hiatuses lasting for 75 to 105 kyr during the intervening interglacial stages. Extension of this pattern to the thin white zone in the interval of beige calcite in the outermost part of the stalagmite suggests an additional brief hiatus early in MIS 6.

4.3. Stable isotope data

Measured values of δ^{13}C from Core CA of the Texas Toothpick range from −8.1 to +1.9‰ relative to the VPDB standard, yielding a range of 10.0‰ that is large compared to ranges reported from other stalagmites (Table 2). Measured values of δ^{18}O range from −9.1 to −4.5‰ relative to VPDB. In data from MIS 8 to MIS 14, values of δ^{13}C and δ^{18}O are commonly highest in samples at the beginnings and ends of marine isotope stages and thus in samples adjacent hiatal surfaces, whereas they are lowest in samples nearer the middles of the glacial intervals (Fig. 7).

Data from MIS 6, from the outermost part of the core, are distinct from data from MIS 8 to 14, from the inner part of the core, in several respects. Values of δ^{13}C from MIS 6 are all higher, values of δ^{18}O are mostly higher, ranges of both δ^{13}C and δ^{18}O are greater, correlation of δ^{13}C and δ^{18}O has a greater value of r^2, and the linear relationship of δ^{13}C to δ^{18}O has a greater slope (Fig. 8). Similarly but less strikingly, among the data from MIS 8 to MIS 14, values of δ^{13}C and δ^{18}O from MIS 8 are generally higher than the average values of δ^{13}C and δ^{18}O from MIS 10 to 14. The origin of this pattern is discussed in Section 5.1.

5. Discussion

5.1. Increasing kinetic fractionation with growth of the Texas Toothpick

Three considerations lead to the conclusion that increased kinetic fractionation accounts for the increase in δ^{13}C and δ^{18}O that is slight

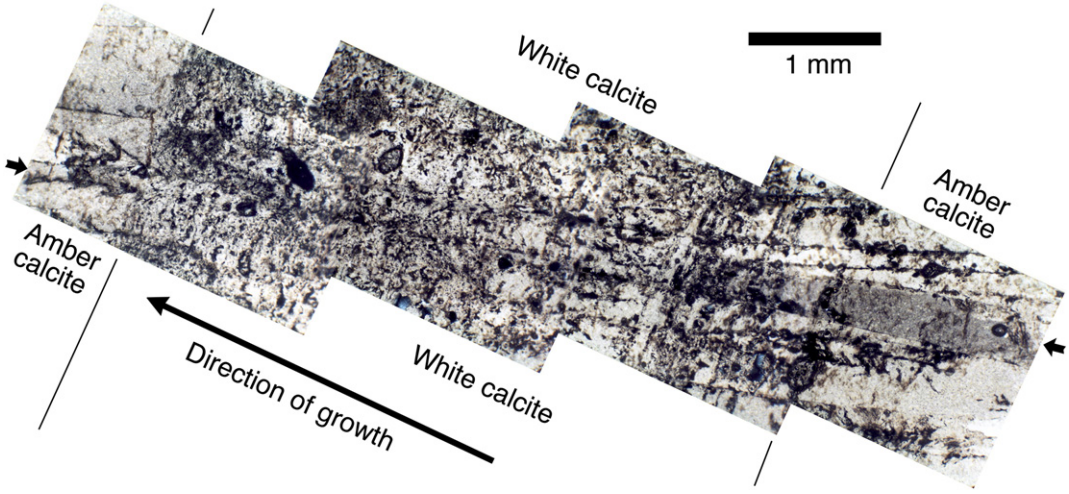

Fig. 4. Mosaic of photomicrographs of one white band in the Texas Toothpick shown in transmitted cross-polarized light. Small arrows point to one crystal that, like many crystals, extends from one amber interval through the white band into the succeeding amber zone. Thin section TTA16.

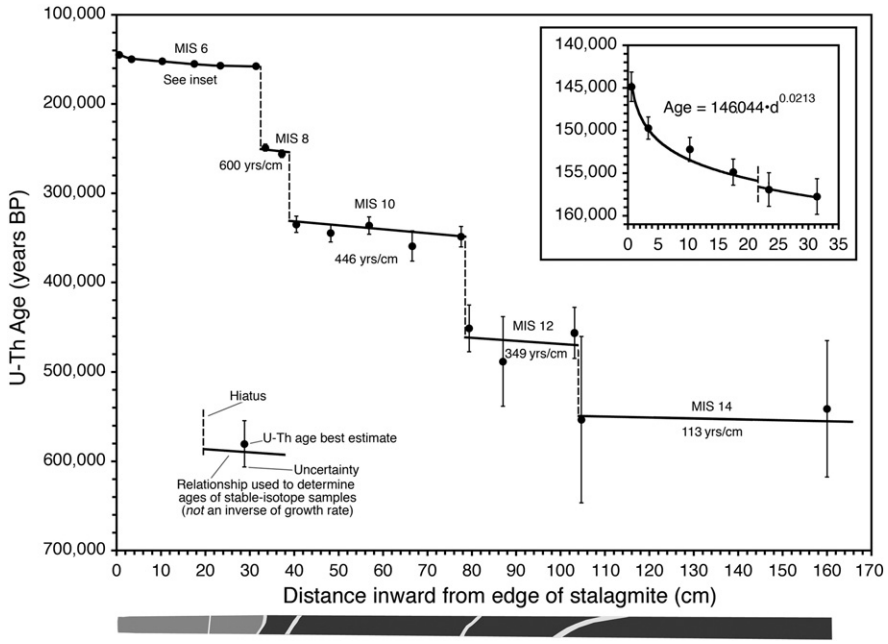

Fig. 5. Age model or chronology for Core CA of the Texas Toothpick stalagmite (specifically, for the left half of the core as seen in Fig. 3). The model is derived from U–Th radiometric ages from brown and beige calcite, whereas ages from the white calcite are not included as they are not thought to be reliable. The schematic diagram at the bottom shows the generalized color of the core, and from left to right one thin white band and four thicker white bands.

but evident in data from MIS 8 and large in data from MIS 6. First, the increasing height of the stalagmite would necessitate that the distance traveled by dripwater from the apex of the stalagmite to the stalagmite's flanks increased, and thus the time for degassing and evaporation increased. Secondly, the decreasing growth rate shown in Fig. 5, both from the center of the stalagmite to its margin and more strikingly in its outermost zone from MIS 6, suggests that the flow of dripwater to any one point on the flanks of the stalagmite decreased through time, consistent with slower flow and greater time for degassing and evaporation from a thinner film of water spread over a larger stalagmite. Thirdly, the absence from Core CA and CC of $CaCO_3$ deposited in MIS 2, the most recent glacial period, suggests that the stalagmite's height ultimately reached a level at which flow to the lower flanks was no longer significant, consistent with a longer-term trend of less flow through time. Thus the markedly higher values of $\delta^{13}C$ and $\delta^{18}O$ from MIS 6 and slightly higher values within MIS 8 than those of previous intervals probably resulted from increasing kinetic fractionation from water traveling farther from the apex and spreading over a larger area of the stalagmite. Such values presumably do not represent long-term changes in climatic conditions from one glacial to the next.

5.2. Wetter glacial stages and drier interglacial stages for 550 ka

5.2.1. Basic interpretation

The clustering of ages from the Texas Toothpick in MIS 6, 8, 10, 12, and 14 suggests sufficient atmospheric precipitation during glacial

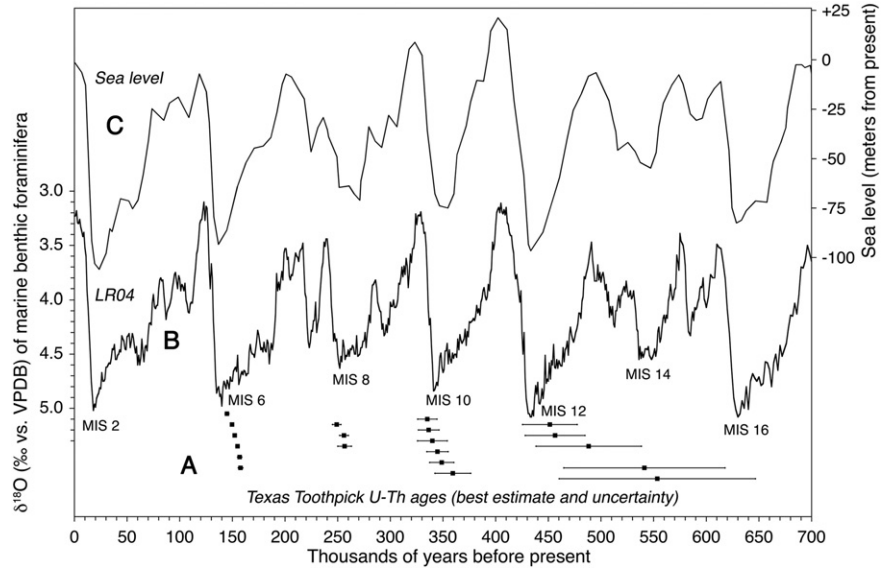

Fig. 6. Texas Toothpick ages compared to sea level and LR04 benthic foraminifera $\delta^{18}O$ data. A. Ages (and their uncertainties) determined from amber and beige calcite of the Texas Toothpick stalagmite (squares and lines). B. The LR04 stack of $\delta^{18}O$ data from the marine benthic foraminifera of Lisiecki and Raymo (2005). C. Sea level, as a consensus of the four different sea level records shown in Fig. 2 of Rohling et al. (2014). Note that the Texas Toothpick ages coincide with maxima (graphic lows) in the LR04 record and with lows in sea level during glacials.

Table 2
Range of $\delta^{13}C$ in stalagmites that have a large range of $\delta^{13}C$.

Stalagmite	Location	Reference	Range of $\delta^{13}C$ (‰)
T8	South Africa	Holmgren et al. (2003)	5.5
–	Belgium	Verheyden et al. (2000)	6.2
GUP	Orissa, India	Yadava and Ramesh (2006)	6.5
Wudu	North-central China	Railsback et al. (2014)	6.8
MC01	Belize	Webster et al. (2007)	7.3
DP1	Namibia	Sletten et al. (2013)	7.4
D4	Southern China	Dykoski et al. (2005)	7.7
CAN	Northern Spain	Moreno et al., (2010)	8.3
SPA121	Austria	Spötl et al. (2008)	8.9
ESP05	Northwestern Spain	Sellers et al. (2013)	9.8
TT	New Mexico, USA	This paper	10.0[a]

[a] Note that this result comes from a horizontal core through a stalagmite, whereas the values above it in the table are all from data collected along the growth axis of stalagmites.

stages to allow water to drip onto the stalagmite and to deposit calcite, whereas the absence of ages from interglacial stages suggests drier periods in which the absence of dripwater prohibited growth of the stalagmite. This interpretation is supported by values of $\delta^{13}C$ and $\delta^{18}O$ that are commonly greatest in samples at the beginnings and ends of glacial stages. Increased values of $\delta^{13}C$ suggest less vegetation and thus less input of ^{13}C-depleted CO_2 into soil water (e.g., Hesterberg and Siegenthaler, 1991; Baldini et al., 2005) and/or more extensive prior carbonate precipitation in a drier cave (Fairchild and McMillan, 2007) and/or more extensive kinetic effects on a drier stalagmite surface. Increased values of $\delta^{18}O$ suggest atmospheric warming, a lessened amount effect, and/or more evaporation (McDermott, 2004; Lachniet, 2009). The data thus combine to suggest drier conditions as deposition began and ended, at the transitions from and to interglacial stages, compared to wetter conditions during the hearts of glacial stages.

One might alternately hypothesize that non-deposition during interglacial periods was the result of conditions too wet to allow supersaturation of dripwater moving across the stalagmite. However, the greater RM of the white bands marking times of non-deposition is best explained by the presence of magnetic particles that settled as dust onto the stalagmite and that would have been washed away if water had moved across the surface (dust commonly moves through the atmosphere of caves and settles on speleothems, as documented in a modern system by Salmon et al. (1995) and inferred in an ancient one by Webster et al. (2007)). Furthermore, the absence of Type E layers, which result from dissolutional erosion (Railsback et al., 2013), argues against flow of dripwater not saturated with respect to calcite. Instead, the relatively diffuse, rather than sharp, nature of the white zones suggests corrosion by condensation from the humid atmosphere of the deep Lower Cave of Carlsbad Cavern during long periods in which no liquid water moved across the stalagmite, and thus during periods of little atmospheric precipitation.

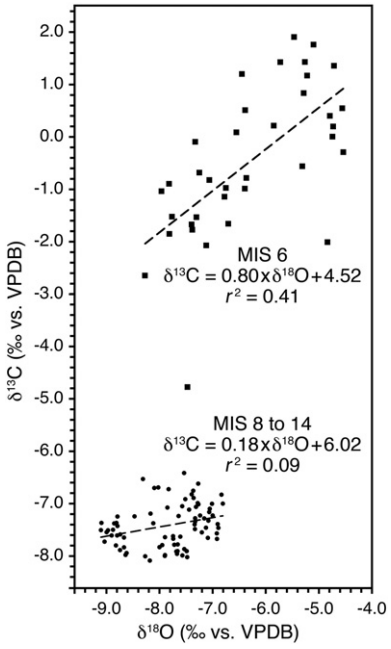

Fig. 8. Plot of carbon and oxygen isotope data from Core CA of the Texas Toothpick stalagmite. Large squares represent data from MIS 6 and thus from the outermost part of stalagmite, whereas small circles represent data from MIS 8 to 14 and thus from the inner part of the stalagmite. Dashed lines are results of linear regressions for which regression equations and values of r^2 are shown. The origin of the patterns seen here is discussed in Section 5.1.

The record from the Texas Toothpick combines with that of another large stalagmite in Carlsbad Cavern, the Georgia Giant, to present an even longer pattern of wetter glacials and drier interglacials. Brook et al. (2006) showed that the Georgia Giant grew during the glacials of MIS 6 and 2, with its lowest values of $\delta^{18}O$ during MIS 6, whereas there was no deposition during the interglacials of MIS 5e and the Holocene, although there was evidence of deposition during other dry intervals (5c and 5a) of MIS 5. The distribution of ages for the Georgia Giant, with gaps in the Holocene and MIS 5e, but with deposition during MIS 2, MIS 3, and MIS 4, suggests a more drought-tolerant stalagmite than the Texas Toothpick, which is in keeping with the Georgia Giant's location in the Green Lake Room, significantly higher in the cave and much closer

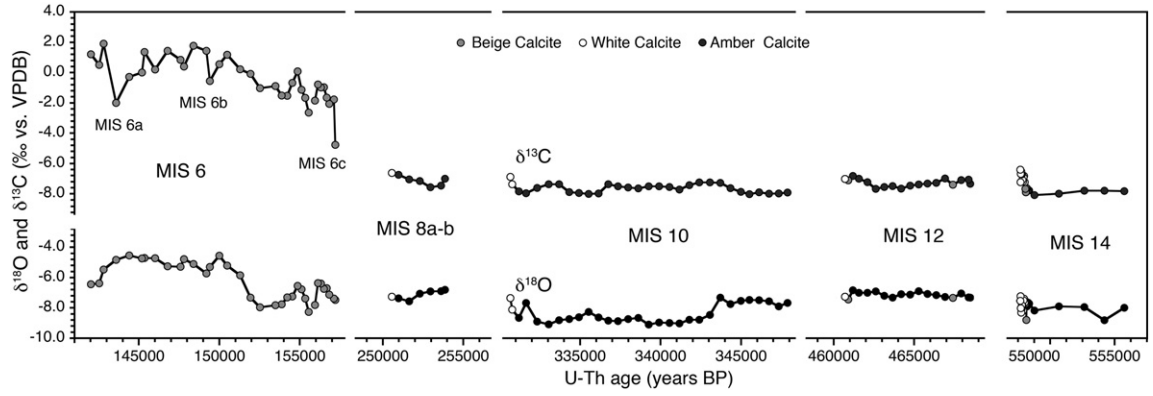

Fig. 7. Carbon and oxygen stable isotope data from core CA of the Texas Toothpick stalagmite (specifically, from the left half of the core as seen in Fig. 3), plotted against ages determined using the age model shown in Fig. 5. Note the breaks in the horizontal time scale. The vertical extent of the symbols exceeds the uncertainty of the $\delta^{13}C$ and $\delta^{18}O$ values. MIS substages are from Railsback et al. (2015).

to the entrance. Thus, if one takes into account the Texas Toothpick's sensitivity to drought and the Georgia Giant's tolerance of drought, they combine to provide a record of wetter glacials and drier interglacials from the Holocene to MIS 14.

5.2.2. Regional climatic relationships in the Quaternary

The wetter glacial stages and drier interglacial stages suggested by the Texas Toothpick and Georgia Giant stalagmites are consistent with other paleoclimate records in the southwestern United States. To the northeast in western Texas, Rich (2013) found no evidence of dune formation in the Last Glacial Maximum but determined that lunette dunes representing drier conditions formed during the Holocene and Sangamonian interglacials. In north-central New Mexico, Polyak and Asmerom (2005) concluded from lacustrine and spelean evidence that the penultimate and last glacials of MIS 6 and 2 were comparatively wet, whereas the interglacials were drier. Farther north and further back in time, Fawcett et al. (2011) concluded from evidence from Valles Caldera in northern New Mexico that comparatively wetter conditions prevailed in the glacials of MIS 10, 12, and 14, whereas "megadroughts" took place in the interglacials of MIS 11 and 13. Farther west in the Great Basin of western Utah and Nevada, Reheis et al. (2014) compiled evidence from ancient shorelines showing that lake levels were higher in many lakes during the Last Glacial Maximum than they are today. Still farther to the west, in southeastern California, Bischoff et al. (1997) found evidence that Owens Lake filled to overflowing during the glacials of MIS 2, 6, 8, 10, and 12 but had no outflow in the interglacials of MIS 5, 7, 9, and 11. Thus records scattered through time and space collectively suggest wetter glacials and drier interglacials across the southwestern United States to complement the Texas Toothpick record (this paper) and Georgia Giant record (Brook et al., 2006) from Carlsbad Cavern extending from MIS 2 back to MIS 14.

The origin of these wetter glacials and drier interglacials in the southwestern United States is commonly attributed to shifts of wind belts equatorward and poleward, respectively, and thus of shifting climatic zones. For example, Metcalfe et al. (2002), Polyak and Asmerom (2005), Brook et al. (2006), and Rich (2013) concluded that southward movement of the westerlies of the polar jet stream, in response to growth of the Laurentide ice sheet, likely accounts for the wetter climate of glacial periods, and Benson et al. (1995) used wetness of Lake Lahontan in western Nevada to map the southern extent of the polar jet stream at the Last Glacial Maximum. Conversely, Fawcett et al. (2011) hypothesized that the intense and prolonged droughts of interglacials resulted from northward expansion of subtropical dry conditions. Carlsbad Cavern is geographically significant to these considerations because it may be near the southern and eastern margins of the influence of the westerlies of the glacial-stage polar jet stream, south of most other sites where influence of the westerlies during glacial stages has been inferred (Fig. 1). Carlsbad's comparatively southern location may be why deposition of the Texas Toothpick was restricted to the coldest parts of glacial stages (i.e., restricted to MIS 6a to 6c but not the warmer Substages 6d and 6e, and restricted to MIS 8a and late 8b but not the warmer substage 8c). However, Metcalfe et al. (2002) did infer the influence of westerlies during the LGM slightly farther south, in the Babicora Basin of northern Chihuahua.

Delivery of more rainfall by westerlies during glacial maxima suggests multiple changes in the climate dynamics of the southwestern United States. Water vapor transported by westerlies during glacials presumably had a source in the northeastern Pacific, rather than an interglacial source in the Gulf of Mexico (as suggested by Feng et al. 2014). Because precipitation from the westerlies typically falls in winter (National Weather Service, 2014; MacMahon and Wagner, 1985, Fig. 5.6), seasonality of rainfall presumably alternated from mostly winter precipitation in glacials to mostly summer precipitation in interglacials like the pattern observed at Carlsbad today. Thus the cycles represented by the Texas Toothpick and Georgia Giant for the most recent 560 kyr suggest alternation between wetter conditions with largely winter rainfall from a Pacific source during glacials to drier conditions with largely summer rainfall derived from the Gulf of Mexico during interglacials.

A westerly source of water vapor delivering mostly winter precipitation during glacials also has implications for the seasonality of recharge, and ultimately for the amount of atmospheric precipitation at Carlsbad. In the Great Basin, where precipitation is more evenly distributed across the year than it is at Carlsbad, groundwater recharge is mostly in the winter months (Harrill and Prudic, 1998; Paul et al., 2014). If the same pattern prevailed at Carlsbad during glacial stages, the greater wetness recorded in the Texas Toothpick stalagmite during those glacial stages could reflect greater recharge during winter months, when evaporation is less than in summer. If so, total annual atmospheric precipitation during "wetter" glacials may not have been significantly greater than in "drier" interglacials, when summer-dominated rainfall underwent more evaporation and thus led to less recharge. In the past decade, paleoclimatologists studying stalagmites have come to recognize that, rather than records of past temperature, stalagmites are more commonly records of "wet and dry periods" (Fairchild and McMillan, 2007), but the scenario of seasonal variation considered here would illustrate the importance of further remembering that stalagmites are more directly records of groundwater recharge than they are records of the amount of atmospheric precipitation.

5.2.3. Further implications of Texas Toothpick $\delta^{18}O$ data

The notion of a westerly source of water vapor during glacials is compatible with the oxygen isotope data from the Texas Toothpick. Lower values of $\delta^{18}O$ in northeastern Pacific seawater compared to those in Gulf of Mexico seawater (LeGrande and Schmidt, 2006) may have contributed to the lower values of $\delta^{18}O$ in Texas Toothpick calcite deposited in the heart of glacial intervals (Fig. 7). However, colder atmospheric temperatures and less extensive evaporation also probably influenced the Texas Toothpick's low values of $\delta^{18}O$.

With regard to the wet glacial periods during which the Texas Toothpick was deposited, it is interesting to note that the thinnest white-bounded amber interval in the Texas Toothpick, and correspondingly the briefest interval of deposition, is that dating to MIS 8. Among the five most recent glacial periods, MIS 8 is the one in which $\delta^{18}O$ values of marine benthic foraminifera in the LR04 record were smallest and thus least strikingly "glacial", and the one in which sea level was highest (Fig. 6). This suggests that the response of atmospheric precipitation in southeastern New Mexico to changing ice volume, and presumably to changing extent of the Laurentide Ice Sheet, was proportional rather than binary, with a lesser shift southward of the polar jet in MIS 8.

5.3. Asynchronicity of signatures of glacial stages, and the extent and volume of ice sheets

Fig. 6 clearly demonstrates that deposition of the Texas Toothpick took place during glacial rather than interglacial stages, but the intervals of Texas Toothpick deposition typically began after the start of glacial stages as shown in the LR04 record and ended before the conclusion of glacial stages as shown in the LR04 record (Table 3). Fig. 5 shows that meaningful ages were recovered near the white hiatal zones of the Texas Toothpick, and thus at the beginnings and ends of intervals

Table 3
Ages of glacial stages as suggested by LR04 and the Texas Toothpick.

Glacial stage	LR04 ages	Texas Toothpick ages	Time missing at start	Time missing at end
MIS 6	191–123 ka	158–145 ka	33 kyr	22 kyr
MIS 8	300–243 ka	257–249 ka	43 kyr	6 kyr
MIS 10	374–337 ka	359–336 ka	15 kyr	0 kyr (−1 kyr)
MIS 12	478–424 ka	488–451 ka	0 kyr (−10 kyr)	27 kyr
MIS 14	563–533 ka	553–541 ka	10 kyr	8 kyr

of deposition, so that the age distribution from the Texas Toothpick is a not an artifact of the sampling interval of Texas Toothpick U–Th age dates. Instead, the discrepancy between ages of glacial stages as seen in the Texas Toothpick in the LR04 record appears to be real. At least two explanations of this discrepancy are possible. One is that the LR04 age model was generated by orbital tuning, specifically by application of a model for volume of glacial ice derived from insolation on 21 June at 65°N (Lisiecki and Raymo, 2005), whereas the Texas Toothpick chronology is based on U–Th ages that might be more representative of actual rather than model global-scale conditions. However, the general concordance of LR04 with other records casts doubt on this explanation. A second explanation is that the two records are records of different things, one a record largely of global volume of glacial ice as indicated by the remains of benthic foraminifera and the other a record of local to regional climate as indicated by calcite deposited from spelean dripwater. This more likely explanation, recognizing that stage and substage boundaries in different records around the world are unlikely to be synchrononous, was discussed in more general terms in Section 5.2 and Fig. 5 of Railsback et al. (2015).

In the specific case of the Texas Toothpick, the discrepancies documented by Table 3 suggest that rainfall sufficient to cause stalagmite deposition took place only in the maxima of glacials, a point supported by comparison of U–Th ages and the LR04 record in Fig. 6, especially with regard to MIS 6, 8, and 10, for which the uncertainties of the U–Th ages are relatively small. The discrepancies in Table 3 do not appear to be the result of a time lag imparted by cave plumbing, because non-deposition is documented at both the beginnings and ends of glacial stages. One possible paleoclimatological inference is that atmospheric precipitation and groundwater recharge *sufficient for deposition of the Texas Toothpick* required that the extent and elevation of the Laurentide Ice Sheet be not only the minimum that is characteristic of a glacial stage, but instead even greater—more like that of a glacial maximum. A second but not contradictory inference might be that the polar jet "squeezed and steered across the continent by high-pressure systems" that prevailed over the North Pacific and over the ice sheet (Oster et al., 2015) may have only supplied rainfall sufficient for deposition of the Texas Toothpick during core intervals of the glacial stages. This would not necessarily mean that there was no rainfall at Carlsbad during the glacial times before and after Texas Toothpick deposition (e.g. 300–257 and 249–243 ka in MIS 8), but only that atmospheric precipitation and groundwater recharge *sufficient for deposition of the Texas Toothpick* were confined to the core interval of the glacial stage (e.g., 257–249 ka in MIS 8).

5.4. Implications for the future

Warming of Earth's climate is now considered "unequivocal" and "unprecedented" compared to past decades to millennia (IPCC, 2013). Within the United States, southeastern New Mexico and most of the U.S. Southwest are in the region of greatest temperature increase in recent decades, and temperatures have increased across all of the western United States (Melillo et al., 2014, Fig. 2.7). If one makes a monotonic extrapolation from the Texas Toothpick's wetter, cooler glacial periods and drier warmer interglacial periods of the past to even warmer conditions expected in the coming century (Melillo et al., 2014, Fig. 20.1), that extrapolation suggests dramatically dry conditions to come (Case A of Fig. 9). This supports others' predictions of lessened water supplies for urban use and agriculture in the U.S. southwest in the 21st century (Melillo et al., 2014, p. 463).

Alternately, one might hypothesize that the broad relationship between temperature and rainfall outlined above is not monotonic and cannot be extrapolated to warm conditions, and that instead the relationship has a reversal involving greater rainfall at temperatures higher than those of the present and past interglacials (Case B of Fig. 9). There is, however, is no evidence to support that hypothesis of a higher-temperature reversal of the general trend. Instead, if one assumes that global-scale warming will lead to northward migration of the Intertropical Convergence Zone and its surrounding climatic zones (as suggested by the last paragraph of Schneider et al. (2014)), then the present rainfall to south (e.g., that of central Chihuahua, where rainfall is about half that at Carlsbad) would support the conclusion that warming would lead to drier conditions in southeastern New Mexico.

6. Conclusions

Radiometric dating of a horizontal core through the lowest part of the massive standing Texas Toothpick stalagmite in Carlsbad Cavern reveals an exceptionally long record of deposition in five successive glacial stages of the Pleistocene, namely MIS 14, 12, 10, 8, and 6. Stable isotope data, measurements of remanent magnetism, and the petrography of the core combine to suggest that the glacial stages were comparatively wetter, whereas the intervening hiatuses represent drier interglacial stages. These results combine with observation of modern climate to suggest alternation between wetter conditions with largely winter rainfall from a Pacific source during glacials to drier conditions with largely summer rainfall derived from the Gulf of Mexico during interglacials. The trend from wetter conditions during colder periods to drier conditions in warmer conditions suggests that atmospheric precipitation and/or groundwater recharge may diminish even more if climate warms in the coming century.

Acknowledgments

This work was partially supported by Grant 2577-82 from the National Geographic Society to BBE and GAB and by Grant NSF 1103320 from the U.S. National Science Foundation to RLE. We are grateful to

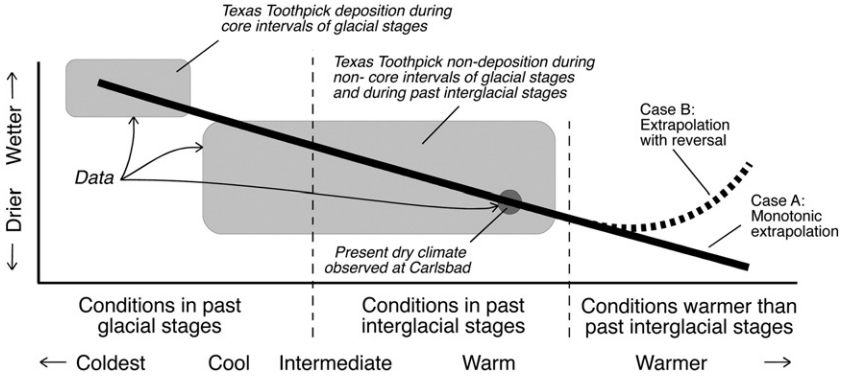

Fig. 9. Schematic representation of possible relationships of rainfall to temperature in southeastern New Mexico through time. The three gray fields represent the observations that constrain two possible relationships between rainfall to temperature, which are represented by the two thick lines, one solid and one dashed. The two extrapolations to warm conditions, which are designated as Case A and Case B, are in the region without gray fields and thus for which there are no constraining observations. Case A and Case B are discussed in Section 5.4.

the National Park Service for allowing the drilling of the two speleothems. Special thanks go to Ron Kerbo, Cave Specialist for the Park Service, for his many hours of help on this project. Also gratefully acknowledged for many hours help in the cave during sampling are Mark Earley and Suzanne, Amber, Robin, and Richard Ellwood. The late Victor Schmidt is gratefully acknowledged for allowing use of his cryogenic magnetometer for the RM measurements. The manuscript was improved by the comments of three *PPP* reviewers, one of whom generated Table 3.

References

Adams, D.K., Comrie, A.C., 1997. The North American Monsoon. Bull. Am. Meteorol. Soc. 78, 2197–2213.

Asmerom, Y., Polyak, V.J., Rasmussen, J.B.T., Burns, S.J., Lachniet, M.S., 2013. Multidecadal to multicentury scale collapses of Northern Hemisphere monsoons over the past millennium. Proc. Natl. Acad. Sci. 110, 9651–9656.

Baldini, J.U.L., McDermott, F., Baker, A., Baldini, L.M., Mattey, D.P., Railsback, L.B., 2005. Biomass effects on stalagmite growth and isotope ratios: a 20th century analogue from Wiltshire, England. Earth Planet. Sci. Lett. 240, 486–494.

Benson, L., Kashagarian, M., Rubin, M., 1995. Carbonate deposition, Pyramid Lake subbasin, Nevada: 2. Lake levels and polar jet stream positions reconstructed from radiocarbon ages and elevations of carbonates (tufas) deposited in the Lahontan basin. Palaeogeogr. Palaeoclimatol. Palaeoecol. 117, 1–30.

Bischoff, J.L., Fitts, J.P., Fitzpatrick, J.A., 1997. Responses of sediment geochemistry to climate change in Owens Lake sediment: an 800 kyr record of saline/fresh cycles. Spec. Pap. Geol. Soc. Am. 317, 37–47.

Black, D.M., 1953. Aragonite rafts in Carlsbad Caverns, New Mexico. Science 117, 84–85.

Brook, G.A., Ellwood, B.B., Railsback, L.B., Cowart, J.B., 2006. A 164 ka record of environmental change in the American Southwest from a Carlsbad Cavern speleothem. Palaeogeogr. Palaeoclimatol. Palaeoecol. 237, 483–507.

Burger, P., 2009. Carlsbad Caverns National Park, New Mexico. U.S. Department of the Interior, National Park Service pamphlet.

Chapman, J.B., Ingraham, N.L., Hess, J.W., 1992. Isotopic investigation of infiltration and unsaturated zone flow processes at Carlsbad Cavern, New Mexico. J. Hydrol. 133, 343–363.

Cheng, H., Edwards, R.L., Hoff, J., Gallup, C.D., Richards, D.A., Asmerom, Y., 2000. The half-lives of uranium-234 and thorium-230. Chem. Geol. 169, 17–33.

Debajyoti, P., Skrzypek, G., 2007. Assessment of carbonate-phosphoric acid analytical technique performed using GasBench II in continuous flow isotope ratio mass spectrometry. Int. J. Mass Spectrom. 262, 180–186.

Douglas, M.W., Maddox, R.A., Howard, K., Reyes, R., 1993. The Mexican Monsoon. J. Clim. 6, 1665–1677.

Dueñas, J.H., 1979. Estudio palinologico de los 3 mts. superiores de la seccion Tarragona, Sabana de Bogota. Caldasia 12, 539–572.

Dykoski, C.A., Edwards, R.L., Cheng, H., Yuan, D.X., Cai, Y.J., Zhang, M.L., Lin, Y.S., An, Z.S., Revenaugh, J., 2005. A high resolution, absolute-dated Holocene and deglacial Asian monsoon record from Dongge Cave, China. Earth Planet. Sci. Lett. 233, 71–86.

Edwards, R.L., Chen, J.H., Wasserburg, G.J., 1987. ^{238}U–^{234}U–230–^{232}Th systematics and the precise measurement of time over the past 500,000 years. Earth Planet. Sci. Lett. 81, 175–192.

Fairchild, I.J., McMillan, E.A., 2007. Speleothems as indicators of wet and dry periods. Int. J. Speleol. 36, 69–74.

Fawcett, P.J., Werne, J.P., Anderson, R.S., Heikoop, J.M., Brown, E.T., Berke, M.A., Smith, S.J., Goff, F., Donohoo-Hurley, L., Cisneros-Dozal, L.M., Schouten, S., Sinninghe Damsté, J.S., Huang, Y., Toney, J., Fessenden, J., WoldeGabriel, G., Atudorei, V., Geissman, J.W., Allen, C.D., 2011. Extended megadroughts in the southwestern United States during Pleistocene interglacials. Nature 470, 518–521.

Feng, W., Hardt, B.F., Banner, J.L., Meyers, K.J., James, E.W., Musgrove, M.L., Edwards, R.L., Cheng, H., Min, A., 2014. Changing amounts and sources of moisture in the U.S. southwest since the Last Glacial Maximum in response to global climate change. Earth Planet. Sci. Lett. 401, 47–56.

Folk, R.L., Assereto, R., 1976. Comparative fabrics of length-slow and length-fast calcite and calcitized aragonite in a Holocene speleothem, Carlsbad Caverns, New Mexico. J. Sediment. Petrol. 46, 486–496.

Gonzalez, L.A., Lohmann, K.C., 1988. Controls on mineralogy and composition of spelean carbonates: Carlsbad Caverns, New Mexico. In: James, N.P., Choquette, P.W. (Eds.), Paloeokarst. Springer-Verlag, New York, pp. 81–101.

Harrill, J.R., Prudic, D.E., 1998. Aquifer systems in the Great Basin region of Nevada, Utah, and adjacent states—summary report: U.S. Geological Survey Professional Paper (1409-A), (66 p.).

Hesterberg, R., Siegenthaler, U., 1991. Production and stable isotope composition of CO_2 in a soil near Bern Switzerland. Tellus 43B, 197–205.

Hill, C.A., 1973. Huntite flowstone in Carlsbad Caverns, New Mexico. Science 181, 158–159.

Holmgren, K., Lee-Thorp, J.A., Cooper, G.R.J., Lundblad, K., Partridge, T.C., Scott, L., Sithaldeen, R., Siep Talmaf, A., Tyson, P.D., 2003. Persistent millennial-scale climatic variability over the past 25,000 years in Southern Africa. Quat. Sci. Rev. 22, 2311–2326.

IPCC, 2013. Summary for Policymakers. In: Stocker, T.F., Qin, D., Plattner, G.-K., Tignor, M., Allen, S.K., Boschung, J., Nauels, A., Xia, Y., Bex, V., Midgley, P.M. (Eds.), Climate Change 2013: The Physical Science Basis. Contribution of Working Group I to the Fifth Assessment Report of the Intergovernmental Panel on Climate Change. Cambridge University Press, Cambridge, United Kingdom and New York, NY, USA.

Lachniet, M.S., 2009. Climatic and environmental controls on speleothem oxygen isotope values. Quat. Sci. Rev. 28, 412–432.

LeGrande, A.N., Schmidt, G.A., 2006. Global gridded data set of the oxygen isotopic composition in seawater. Geophys. Res. Lett. 33, L12604. http://dx.doi.org/10.1029/2006GL026011.

Lisiecki, L.E., Raymo, M.E., 2005. A Pliocene–Pleistocene stack of 57 globally distributed benthic $\delta^{18}O$ records. Paleoceanography 20. http://dx.doi.org/10.1029/2004PA001071.

MacMahon, J.A., Wagner, F.H., 1985. The Mojave, Sonoran and Chihuahuan Deserts of North America. In: Evenari, M., Noy-Meir, I., Goodall, D.W. (Eds.), Ecosystems of the World. Elsevier, Amsterdam, pp. 105–202.

McDermott, F., 2004. Palaeo-climate reconstruction from stable isotope variations in speleothems: a review. Quat. Sci. Rev. 23, 901–918.

Melillo, J.M., Richmond, T.C., Yohe, G.W., 2014. Climate Change Impacts in the United States: The Third National Climate Assessment. U.S. Global Change Research Program. http://dx.doi.org/10.7930/JOZ31WJ2 (841 p.).

Metcalfe, S., Say, A., Black, S., McCulloch, R., O'Hara, S., 2002. Wet conditions during the last glaciation in the Chihuahuan Desert, Alta Babicora Basin, Mexico. Quat. Res. 57, 91–101.

Moreno, A., Stoll, H., Jiménez-Sánchez, M., Cacho, I., Valero-Garcés, B., Ito, E., Edwards, R.L., 2010. A speleothem record of glacial (25–11.6 kyr BP) rapid climatic changes from northern Iberian Peninsula. Glob. Planet. Chang. 71, 218–231.

National Weather Service, 2014. NOWData—NOAA Online Weather Data. www.nws.noaa.gov/climate/xmacis.php?wfo = mfr accessed 26 October 2014.

Oster, J.L., Ibarram, D.E., Winnick, M.J., Maher, K., 2015. Steering of westerly storms over western North America at the Last Glacial Maximum. Nat. Geosci. 8, 201–205.

Paul, A.P., Thodal, C.E., Baker, G.M., Lico, M.S., Prudic, D.E., 2014. Preliminary geochemical assessment of water from selected streams, springs, and caves in the Upper Baker and Snake Creek drainages in Great Basin National Park, Nevada, 2009. U.S. Geological Survey, Scientific Investigations Report 2014-5108 (33 p.).

Polyak, V.J., Asmerom, Y., 2001. Late Holocene climate and cultural changes in the southwestern United States. Science 294, 148–151.

Polyak, V.J., Asmerom, Y., 2005. Orbital control of long-term moisture in the southwestern USA. Geophys. Res. Lett. 32, L19709. http://dx.doi.org/10.1029/2005GL023919.

Polyak, V.J., Rasmussen, J.B.T., Asmerom, Y., 2004. Prolonged wet period in the southwestern United States through the Younger Dryas. Geology 32, 5–8.

Polyak, V.J., Asmerom, Y., Burns, S.J., Lachniet, M.S., 2012. Climatic backdrop to the terminal Pleistocene extinction of North American mammals. Geology 40, 1023–1026.

Railsback, L.B., 2015. Diminishing Knowledge with Increasing Age Through Quaternary Time, *in* Fundamentals of Quaternary Science (www.gly.uga.edu/railsback/FQS/FQS.html).

Railsback, L.B., Akers, P.D., Wang, L., Holdridge, G.A., Voarintsoa, N., 2013. Layer-bounding surfaces in stalagmites as keys to better paleoclimatological histories and chronologies. Int. J. Speleol. 42, 167–180.

Railsback, L.B., Xiao, H., Liang, F., Akers, P.D., Brook, G.A., Dennis, W.M., Lanier, T.E., Cheng, H., Edwards, R.L., 2014. A stalagmite record of abrupt climate change and possible Westerlies-derived atmospheric precipitation during the Penultimate Glacial Maximum in northern China. Palaeogeogr. Palaeoclimatol. Palaeoecol. 393, 30–44.

Railsback, L.B., Gibbard, P.L., Head, M.J., Voarintsoa, N.R.G., Toucanne, S., 2015. An optimized scheme of lettered marine isotope substages for the last 1.0 million years, and the climatostratigraphic nature of isotope stages and substages. Quat. Sci. Rev. 111, 94–106.

Reheis, M.C., Adams, K.D., Oviatt, C.G., Bacon, S.N., 2014. Pluvial lakes in the Great Basin of the western United States—a view from the outcrop. Quat. Sci. Rev. 97, 33–57.

Rich, J., 2013. A 250,000-year record of lunette dune accumulation on the Southern High Plains, USA and implications for past climates. Quat. Sci. Rev. 62, 1–20.

Rohling, E.J., Foster, G.L., Grant, K.M., Marino, G., Roberts, A.P., Tamisiea, M.E., Williams, F., 2014. Sea-level and deep-sea-temperature variability over the past 5.3 million years. Nature 508, 477–482.

Salmon, L.G., Christoforou, C.S., Gerk, T.J., Cass, G.R., Cassucio, G.S., Cooke, G.A., Leger, M., Olmez, I., 1995. Source contributions to airborne particle deposition at the Yungang Grottoes, China. Sci. Total Environ. 167, 33–47.

Schneider, T., Bischoff, T., Haug, G.H., 2014. Migrations and dynamics of the intertropical convergence zone. Nature 513, 45–53. http://dx.doi.org/10.1038/Nature13636.

Sellers, R., Railsback, L.B., Liang, F., Vidal Romani, J.R., Vaquero, M., Grandal, A., Edwards, R.L., Cheng, H., 2013. Isotopic and Petrographic Evidence for Quaternary Long-Term Climate Change from a Stalagmite from the Serra do Courel of Spain. Abstract, Geological Society of America Annual Meeting, Denver, Colorado (October 2013).

Shen, C.C., Edwards, R.L., Cheng, H., Dorale, J.A., Thomas, R.B., Moran, S.B., Weinstein, S.E., Edmonds, H.N., 2002. Uranium and thorium isotopic and concentration measurements by magnetic sector inductively coupled plasma mass spectrometry. Chem. Geol. 185, 165–178.

Sletten, H.R., Railsback, L.B., Liang, F., Brook, G.A., Marais, E., Hardt, B.F., Cheng, H., Edwards, R.L., 2013. A petrographic and geochemical record of climate change over the last 4600 years from a northern Namibia stalagmite, with evidence of abruptly wetter climate at the beginning of southern Africa's Iron Age. Palaeogeogr. Palaeoclimatol. Palaeoecol. 376, 149–162.

Spötl, C., Scholz, D., Mangini, A., 2008. A terrestrial U/Th-dated stable isotope record of the Penultimate Interglacial. Earth Planet. Sci. Lett. 276, 283–292.

Sun, Y., Clemens, S.C., An, Z., Yu, Z., 2006. Astronomical timescale and palaeoclimatic implication of stacked 3.6-Myr monsoon records from the Chinese Loess Plateau. Quat. Sci. Rev. 25, 33–48.

Thrailkill, J., 1968. Dolomite cave deposits from Carlsbad Caverns. J. Sediment. Res. 38, 141–145.
Thrailkill, J., 1977. Carbonate deposition in Carlsbad Caverns. J. Geol. 79, 683–695.
Tzedakis, P.C., Hooghiemstra, H., Pälike, H., 2006. The last 1.35 million years at Tenaghi Philippon: revised chronostratigraphy and long-term vegetation trends. Quat. Sci. Rev. 25, 3416–3430.
Verheyden, S., Keppens, E., Fairchild, I.J., McDermott, F., Weis, D., 2000. Mg, Sr and Sr isotope geochemistry of a Belgian Holocene speleothem: implications for paleoclimate reconstructions. Chem. Geol. 169, 131–144.
Wang, P.X., 2009. Global monsoon in a geological perspective. Chin. Sci. Bull. 54, 1113–1136.
Webster, J.W., Brook, G.A., Railsback, L.B., Cheng, H., Edwards, R.L., Alexander, C., Reeder, P.R., 2007. Stalagmite evidence from Belize indicating significant droughts at the time of Preclassic Abandonment, the Maya Hiatus, and the Classic Maya Collapse. Palaeogeogr. Palaeoclimatol. Palaeoecol. 250, 1–17.
Yadava, M.G., Ramesh, R., 2006. Stable oxygen and carbon isotope variations as monsoon proxies: a comparative study of speleothems from four different locations in India: Journal of the Geological Society of India 68, 461–475.